PAPER

Interface imperfection effects on spin transfer torque switching: an atomistic approach

To cite this article: Akhil K Ramesh *et al* 2022 *J. Phys. D: Appl. Phys.* **55** 215002

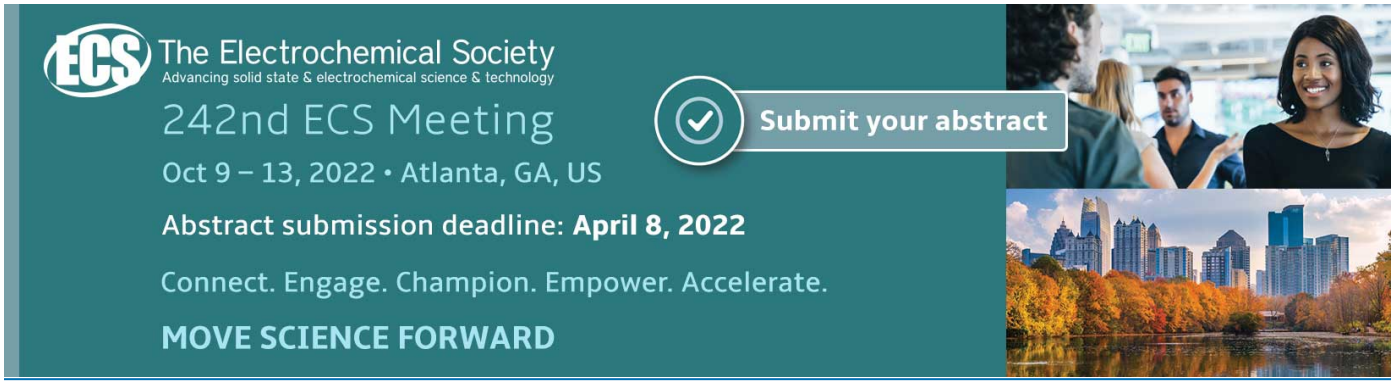

IOP Publishing Journal of Physics D: Applied Physics
J. Phys. D: Appl. Phys. **55** (2022) 215002 (7pp) https://doi.org/10.1088/1361-6463/ac55c2

Interface imperfection effects on spin transfer torque switching: an atomistic approach

Akhil K Ramesh[1,2], Chih-Wei Cheng[1], Ting-Chia Ku[1], Vaibhav Rana[2], Pratisha Gangwar[2], Pushparaj Singh[2] and Yuan-Chieh Tseng[1,*]

[1] Department of Materials Science and Engineering, National Yang Ming Chiao Tung University, Hsinchu, Taiwan
[2] Centre for Applied Research in Electronics (CARE), Indian Institute of Technology Delhi, India

E-mail: yctseng1978@nycu.edu.tw

Received 9 December 2021, revised 2 February 2022
Accepted for publication 16 February 2022
Published 28 February 2022

Abstract

The further commercialization of spintronic memory devices depends on the development of methods by which to assess performance. This paper presents an approach to the atomistic investigation of switching performance in spin transfer torque magneto-resistive random access memory (MRAM) devices with the use of interface imperfection model. Switching simulation in the nanosecond regime was made possible under this model, and we first time demonstrate that switching time is inversely proportional to interface imperfection (i.e. roughness). In investigating the damping of CoFeB/MgO films, we analyzed the effective damping constant α_{eff}, which cannot be accurately predicted for ferromagnetic layers of less than 2 nm using existing micromagnetic models. The proposed model includes a roughness parameter, which has nearly no effect on the effective damping constant in films of >2 nm, but a profound effect in films of <2 nm, reaching a 27% decrease in a 1.0 nm CoFeB film. Our finding is supported by the experimental data of classic references. We expect that these results will prove valuable in magnetic simulation and research on MRAM with ultrathin films.

Keywords: spintronics, atomistic modeling, micromagnetic simulation, switching current density, spin transfer torque magnetic random access memory (STT-MRAM)

(Some figures may appear in color only in the online journal)

1. Introduction

Research in memory technology focuses primarily on reducing power consumption and increasing read/write speeds without compromising reliability. Magneto-resistive random access memory (MRAM) is currently the best candidate for high-speed nonvolatile memory devices in high density arrays with low power consumption and decent thermal stability [1, 2]. Magnetic tunnel junctions (MTJs), in which an insulator barrier is sandwiched between two ferromagnetic layers, is at the heart of MRAM technology [3, 4], and has proven particularly effective in tunnel magnetoresistive devices and circuits [5, 6]. Spin transfer torque (STT)-MRAM devices with a CoFeB/MgO/CoFeB heterostructure provide high thermal stability and a low damping constant [7]. The data retention of commercial 1 GB MRAM devices has been estimated at 20 years at 105 °C, during which they are expected to provide reliable STT switching with a pulse width of less than 10 ns [8]. Most of the underlying advances can be attributed to research on the CoFeB/MgO interface and the introduction of perpendicular (p) MTJ [9, 10]. Advances in manufacturing have reduced the device size from 100 nm to less than 50 nm; however, miniaturization has also introduced problems related

* Author to whom any correspondence should be addressed.

to dielectric breakdown, etching damage, stray fields, and interface effects (e.g. boron diffusion) [11]. Numerous methods have been suggested to study performance issues related to interface effects [12, 13]. Note however that MRAM performance also depends on the physical properties and magnetization dynamics of the constituent magnetic materials [14]. Roughness at the CoFeB/MgO interface is a key parameter affecting electrical reliability [15]. Micromagnetic simulation is based on the Landau–Lifshitz–Gilbert (LLG) equation used in conjunction with the finite element method to simulate phenomena at the 'mesoscopic' scale [16]. However, at the nanometer scale, MRAM film layering becomes increasingly complex, with a corresponding increase in the computational overhead involved in micromagnetic simulation. Engineering at these scales must account for process variation and a range of device properties (e.g. interface roughness, interface diffusion, array shape, and operating temperature). Atomic-level magnetic simulation can be used to address phenomena at sub-nanometer scales. It can also be used to simulate the complex exchange of energy in the lattice systems of anti-ferromagnetic materials. The computational burden of atomic-level magnetic simulation is far lower than that of the grid scheme used in the finite element method, which must account for the atomic-level magnetic moment at every lattice point. Atomic-level magnetic simulation is also applicable to many systems that cannot be simulated using conventional micromagnetic software, such as the crystal lattices and interfaces associated with MRAM components.

In this study, we employed Vampire simulation software [17] to construct an atomistic model of the CoFeB ferromagnetic layer for use in studying the effects of interface roughness on dynamic magnetic characteristics. In typical MTJ structures, many factors can affect interface roughness, including film design, layer insertion, sputtering parameters, and annealing parameters [18–20]. Furthermore, when the device size is reduced and/or the film thickness is decreased, the effect of roughness on device performance increases dramatically.

In Park *et al* [15], they studied the effect of roughness on the electrical performance of MTJs; however, they did not account for magnetic properties. In Chureemart *et al* [21], they performed an atomistic investigation of the magnetic properties of MTJ (e.g. damping constant); however, roughness was not taken into account [21]. In the current study, we established a new approach to the atomistic simulation of MTJs, which accounts for the effects of roughness [22] as well as the damping constant [21] when addressing switching performances in STT-MRAM.

In section 2, we detail the proposed roughness model for atomistic simulation. We then describe how the damping constant (as a function of roughness) is used to derive the switching time and switching current density. Finally, our results are compared with those obtained in an atomistic study of the damping constant as a function of thickness by Chureemart *et al* [21] (theory) and switching current estimates by Ikeda *et al* [23] (experiment).

2. Simulation

The choice of materials for the tunneling layer and the ferromagnetic layer can greatly affect the switching performance of p-MTJs. Growing a high-quality MgO layer with a (001) crystal lattice direction, and ensuring that the amorphous CoFeB layer crystallizes near the MgO after annealing both require a smooth ferromagnet-insulator interface. Roughness at the interface reduces the tunneling magneto-resistance of p-MTJs, leading to a reduction in breakdown voltage (breakdown voltage) and device reliability. Note however that increasing roughness at the interface can also affect interface anisotropy and enable faster switching. This imposes a trade-off between the performance parameters of p-MTJs [13]. In the atomistic simulation of roughness, magnetic properties are assigned separately for bulk CoFeB and the CoFeB interface.

In the current study, roughness was included in the damping test using the built-in Vampire roughness function [22], which generates a specific number of seed points on a particular height plane. The simulator inputs the number of lattice points, and the method of selection involves random number generation. Neighboring atoms are adjusted according to these established points to generate peaks and troughs, as shown in figure 1. This model does not alter the position of lattice points, but rather uses it to select and replace atoms in order to simulate the effects of roughness. Due to the extreme thinness of the film, we limited atom substitution to two atomic layers to avoid the effects of diffusion. Note also that the average roughness (R_a) does not provide a good description of surface morphology; therefore, we selected root-mean-square roughness R_q as the parameter by which to quantify roughness, as follows:

$$R_q = \sqrt{\frac{1}{N}\sum_{i=1}^{N}(Z_i - Z_a)^2}. \quad (1)$$

Essentially, we derive the root mean square value from the Z coordinates of all CoFeB (i.e. interface) atoms (Z_i) after substitution. The extremely limited atomic substitution minimized the effect on R_{max}, such that the resulting model is applicable only to film thicknesses of less than 2 nm. As shown in figures 1(a) and (b), roughness R_q was adjusted by increasing the number of seed points, while maintaining the uniformity of the film. This approach maintained the average coordinates at the CoFeB interface (Z_a) at close to the original plane, while avoiding average plane displacement. Taken together, this created a situation similar to the displacement of interface membranes.

To validate the proposed roughness model, we compared changes in magnetic properties as a function of CoFeB free layer thickness (<2 nm) with the results obtained in [21, 23]. As shown in figure 2(a), the number of seed points was correlated directly with roughness. Figure 2(b) is the schematic illustration of roughness variation with seed points. The simulation results can be analyzed through the visualization of atoms using open source software, such as Jmol and POV-Ray.

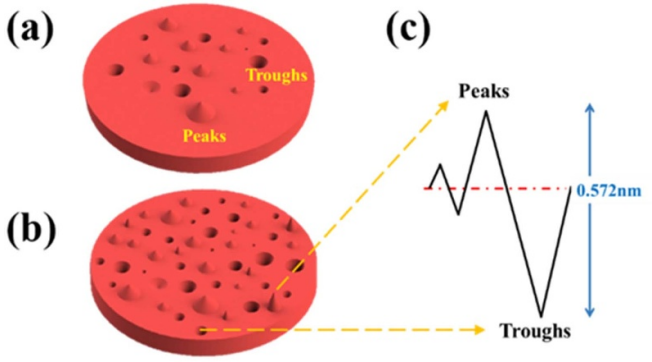

Figure 1. Schematic illustration showing our model containing the effects of roughness: (a) and (b) peaks and troughs; (c) R_{max} did not exceed two atomic layers to prevent extreme values from affecting the simulation results, and to prevent effects similar to those of diffusion.

Note that our investigation of the CoFeB/MgO interface in this paper was based on a number of assumptions. In accordance with [23], we assumed that the perpendicular magnetic anisotropy (PMA) of CoFeB was derived from the interface that formed after annealing with MgO, and that the magnetic properties of the region near the MgO differed from those in other regions of the film. We assumed that the CoFeB interface had high anisotropic energy and high exchange energy. We also assumed that the CoFeB interface possessed a good body center cubic (BCC) structure, regardless of the interface and bulk crystal lattice. We considered only the interface between CoFeB/MgO on one side. On the other side, we considered only the loss of coordination number.

Atomistic simulation was used to study magnetization dynamics. Damping constant α is an extremely important parameter in the LLG equation. The initial value was set at 0.01 (based on previous reports [21]); however, the damping constant can be affected by a variety of external factors. Thus, we obtained the actual α_{eff} using damping test simulations followed by reverse inference. We set the initial magnetic moment of the film at 30° from the $+Z$ axis and applied an external magnetic field H_{ext}, =5 T in the $+Z$ direction. As the field is applied, the magnetic moment will start processing around the external field with gradually reducing amplitude until it finally gets aligned along the $+Z$ direction. This happens because a magnetic sample under an applied field with the magnetization vector $\mathbf{S}_i$ and applied equivalent field H_{ext} in different directions, the magnetic moment moves in precession mode under the effects of damping toward the direction of the applied equivalent field. We are providing a condition such that the precision cone is making an angle of 30° with the $+Z$ axis. Under these damping conditions, time-dependent variations in the magnetic moments in the *x*, *y*, and *z* directions can be represented using the standard LLG equation [24], as follows:

$$\frac{\partial \mathbf{S}_i}{\partial t} = \frac{\gamma}{(1+\propto^2)}\left[\mathbf{S}_i \times \mathbf{H}^i_{\text{eff}} + \propto \mathbf{S}_i \times \left(\mathbf{S}_i \times \mathbf{H}^i_{\text{eff}}\right)\right] \quad (2)$$

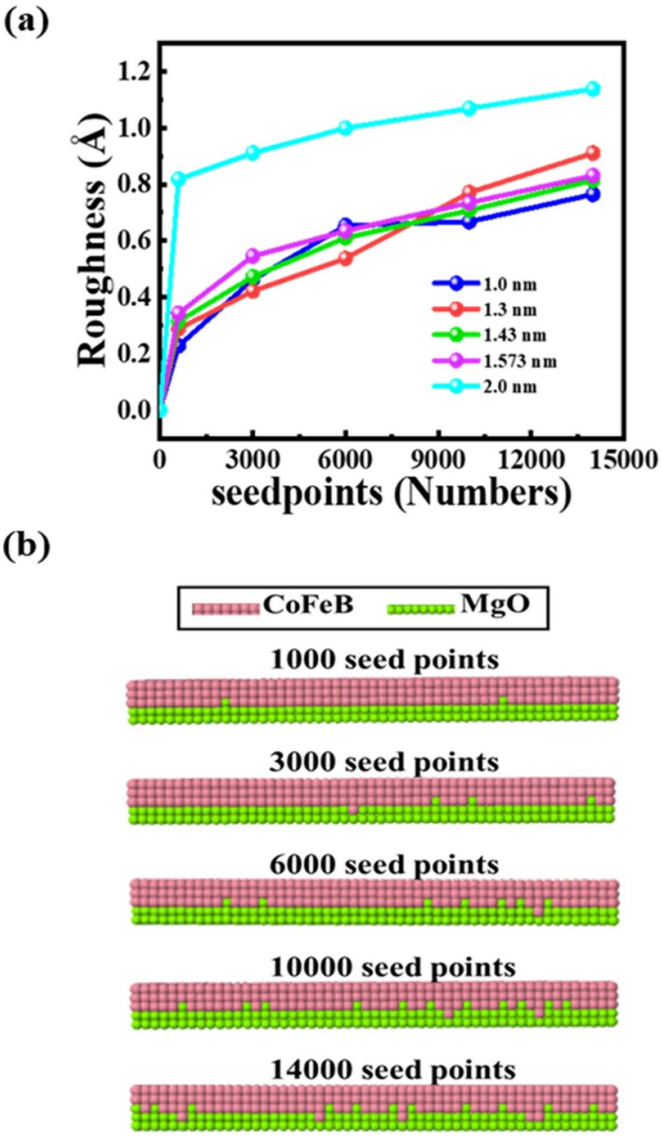

Figure 2. (a) Comparison of roughness (determined by the number of seed points) in CoFeB free layers (FLs) of various thicknesses (b) schematic illustration of interface roughness variation with respect to seed points.

where $\mathbf{S}_i$ is the unit vector of the magnetic moment of an individual atom; γ is the gyromagnetic ratio; $\mathbf{H}^i_{\text{eff}}$ is the effective field experienced by individual atoms, and α is the Gilbert damping constant. The effective field can be written as follows:

$$\mathbf{H}^i_{\text{eff}} = -\frac{1}{\mu_s}\frac{\partial \hat{H}}{\partial \mathbf{S}_i} \quad (3)$$

where $\hat{H}$ indicates the spin Hamiltonian [15]. Under the macrospin model in which a magnet is regarded as a macroscopic magnetic moment, the analytical solution of the LLG equation can be written as follows:

$$S_x(t) = \text{sech}\left(\frac{\propto \gamma H}{1+\propto^2}\right)\cos\left(\frac{\gamma H}{1+\propto^2}t\right) \quad (4)$$

Table 1. Atomistic simulation parameters.

Parameter	$CoFeB_{bulk}$	$CoFeB_{interface}$	Unit
Lattice constant	2.86	2.86	Å
Exchange constant	7.735×10^{-21}	1.547×10^{-20}	J link^{-1}
Spin magnetic moment	1.6	1.6	μ_B
K_u	0.5×10^{-32}	1.35×10^{-22}	J atom^{-1}
Initial damping constant	0.003	0.11	Non

$$S_y(t) = \operatorname{sech}\left(\frac{\propto \gamma H}{1+\propto^2}\right)\sin\left(\frac{\gamma H}{1+\propto^2}t\right) \quad (5)$$

$$S_z(t) = \tanh\left(\frac{\propto \gamma H}{1+\propto^2}t\right). \quad (6)$$

The α_{eff} value obtained by fitting the results to equation (6) of damping test is used in the macrospin model to obtain the magnetization in *x, y* and *z* directions. In the damping test, magnetic moment change (M_t) shows the precession behavior and follows the analytical solution of LLG equation, which can be summarized in the macrospin model:

$$M_t = A \cdot \exp\left(\frac{t}{\tau}\right)\cos(2\pi f t) \quad (7)$$

where A is the amplitude, f is the frequency, and τ is the relaxation time. The atomistic simulation was performed by considering the bulk and interface as two independent materials within the BCC lattice [25], and the simulation parameters are summarized in table 1.

Constrained Monte Carlo (CMC) [26] simulation was used to obtain the equilibrium quantities and anisotropy energy by which to derive differences in energy between magnetization states oriented in different directions. Note that anisotropy energy is derived from torque. CMC simulation was used to constrain the direction of global magnetization, while allowing the single spin to vary [27], thereby making it possible to calculate the restoring torque acting on magnetization. The energy of the system was calculated in accordance with the methods in [26].

We performed micromagnetic simulations using the object-oriented micromagnetic framework (OOMMF) to determine the switching current density [28, 29]. The roughness variation was incorporated to OOMMF based on the corresponding variation in damping constant. Here, the parameters of the free layer were optimized via atomistic simulation and the parameters of the fixed layer were based on the findings in [30]. The saturation magnetization assigned was 1.1×10^6 A m^{-1} and the spin-torque efficiency used is 0.7. We used micromagnetic simulation to estimate the minimum switching current density required for nanosecond switching. Under a fixed current, we then studied the variations in switching time across a range of damping constant values corresponding to roughness values for a free layer with a thickness of 1.3 nm.

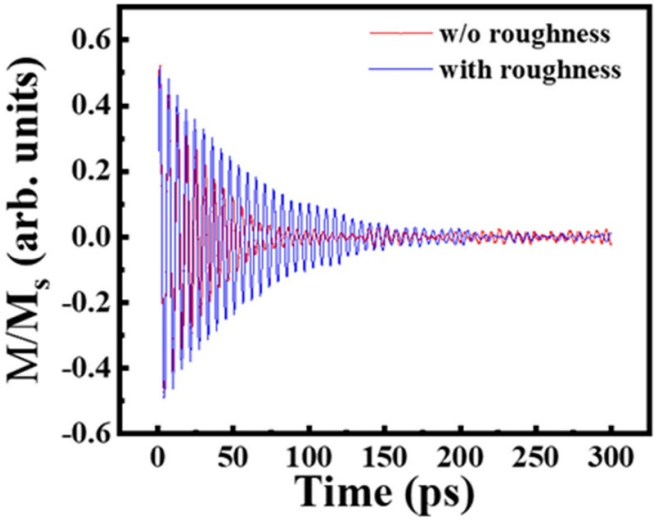

Figure 3. Comparison of damping results between the roughness system and the original system, where the thickness of the ferromagnetic layer was 1.3 nm.

3. Results and discussion

This series of simulations involved a circular film (40 nm in diameter) under an applied external magnetic field of 5 T. Precession behavior in the damping test should be more precise; therefore, we set each time step at 0.5 ps in the VAMPIRE simulation. The temperature was set at 5 K to minimize temperature effects. As shown in figure 3, under a given set of parameters, the precession of the roughness system differed from that of the original system. Differences in the effective damping constant inevitably affect the flipping behavior of the magnetic film. To facilitate comparisons with the results reported in the literature, we performed simulations using a variety of roughness values and CoFeB thicknesses.

The thickness of CoFeB supporting PMA is generally 1.3–1.7 nm, and researchers have previously reported that films exceeding 2 nm in thickness present in-plane behavior [19]. Thus, we conducted simulations using films of various roughness, where the film thickness was limited to less than 2 nm. When roughness was omitted, the damping constant was inversely proportional to thickness as well as roughness (see figure 4(a)). Note however that the effect of roughness on the damping constant eventually plateaued. Moreover, roughness had very little effect on the effective damping constant of thin films (>2 nm), which is in line with the results in the literature [21, 23], as shown in figure 4(b). Increasing the film thickness to 1.0 nm reduced the effective damping constant by 27%. We obtained a damping constant close to the experimental values using a film thickness of 1.3 nm and roughness $R_q = 0.3$ Å [23].

Nevertheless, a lack of empirical data related to roughness made it difficult to perform accurate comparisons. Thus, we sought to validate the proposed model by comparing the current density required to switch from parallel to antiparallel (P to AP) and antiparallel to parallel (AP to P) via micromagnetic simulation. We used the damping constant obtained

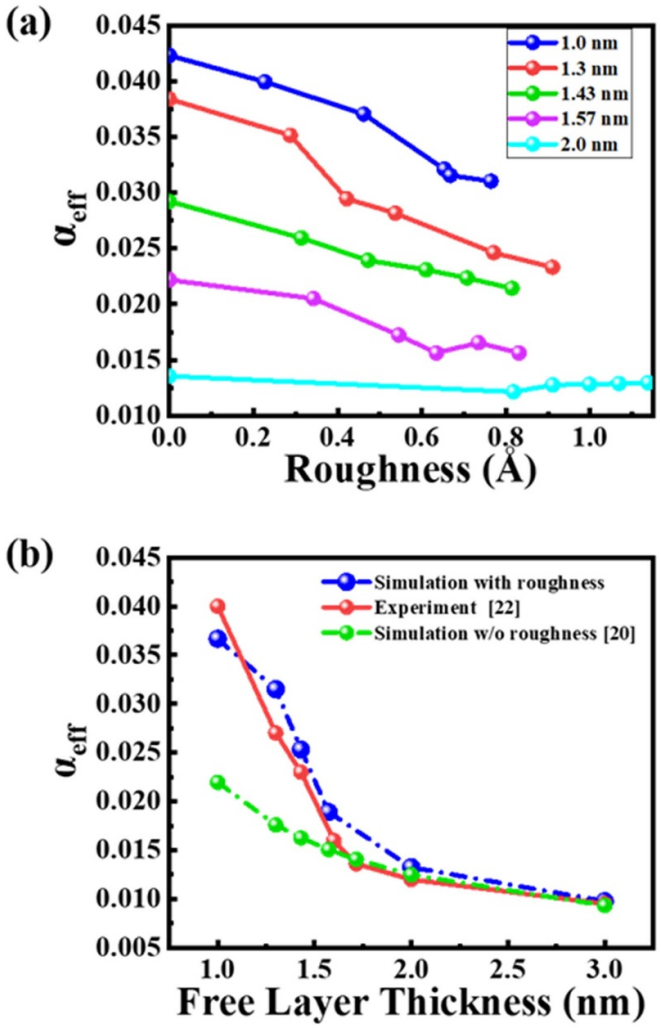

Figure 4. (a) Effective damping constant (α_{eff}) as a function of R_{q} and CoFeB thickness; (b) comparison of damping constant as a function of roughness in previous theoretical [21] and experimental [23] studies.

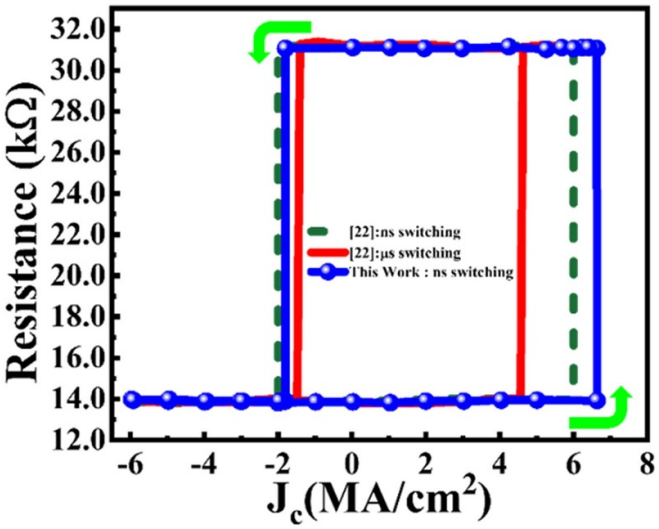

Figure 5. Resistance versus applied current density (*R–J* curves): experimental data and predicted values.

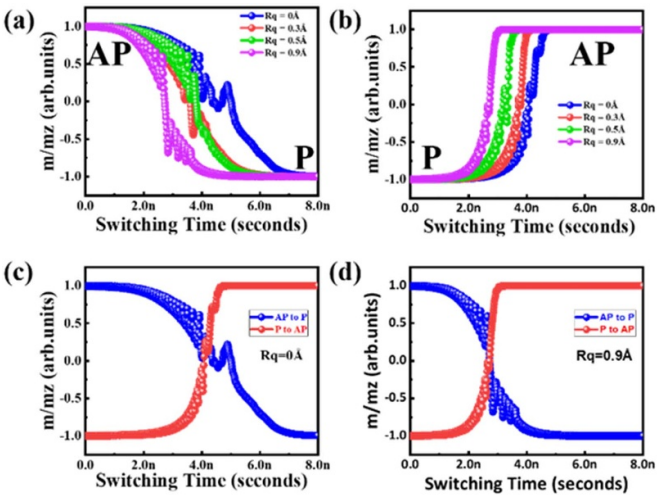

Figure 6. Graphs showing switching times under various roughness values: (a) AP to P; and (b) P to AP. A difference of 1 ns was observed between (c) minimum roughness and (d) maximum roughness.

at $R_{\text{q}} = 0.3$ Å for the micromagnetic simulation, due to the fact that we obtained the best fit between simulation and experimental data at this roughness with $\alpha = 0.003\,55$ (see figure 4(b)). The switching current required for AP $\rightarrow$ P was $J_{\text{c}} = -1.8$ MA cm^{-2}, whereas the switching current for P $\rightarrow$ AP transitions was $J_{\text{c}} = 6.6$ MA cm^{-2}. Clear switching behavior was observed when using resistance values corresponding to high- (AP) and low-resistance (P) states for p-MTJ with diameter 40 nm [23], as indicated by the *R–J* curves in figure 5. The current density required for nanosecond (300 μs) switching was roughly $J_{\text{c}} = -2$ MA cm^{-2} from AP to P and $J_{\text{c}} = 6.0$ MA cm^{-2} from P to AP, as derived using the current-induced magnetization switching equation, as follows:

$$I_{\text{c0}} = 2\alpha E \frac{\gamma e}{\mu_{\text{B}} g} \tag{8}$$

where e indicates the elementary charge, μ_{B} is the Bohr magneton, and g is a function of the angle between the magnetizations of the free and reference layers [31]. The current density values obtained using current induced magnetization switching approximation are very close to those obtained using micromagnetic simulations based on roughness.

We fixed the current density at $J_{\text{c}} = -1.8$ MA cm^{-2} in order to study switching from AP to P under a range of roughness values ($R_{\text{q}} = 0$, 0.3, 0.5 and 0.9 Å). Overall, switching time was inversely proportional to roughness. We also studied switching from P to AP under low, moderate, and high roughness values. Again, switching time was inversely proportional to roughness, as shown in figures 6(a) and (b). Note that switching times varied by 1 ns between minimum and maximum roughness conditions, as shown in the figures 6(c) and (d).

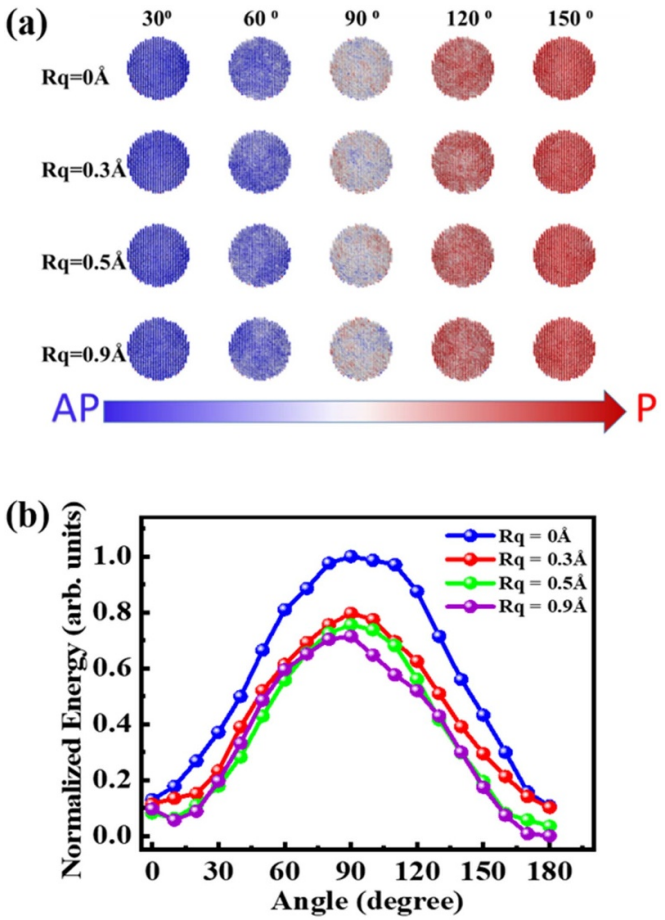

Figure 7. Switching from an AP to a P state using CMC simulation in VAMPIRE: (a) the number of atoms that switched to 90° was positively correlated with the degree of roughness; (b) the energy barrier was inversely correlated with roughness.

CMC simulation was used to characterize the variations in atomic spin as a function of roughness based on the seed point parameter. As shown in figure 7(a), spin configuration at atomic level was successfully monitored during reversal while changing roughness. Again, this indicates that switching speed was proportional to roughness. As shown in figure 7(b), the energy barrier to be crossed when switching from AP to P increased with a decrease in roughness. The reduction in energy barrier can be observed as a reduction in switching time under current density of $J_c = -1.8$ MA cm^{-2}. In summary, roughness was shown to promote current induced magnetization switching, due to variations in anisotropy, as suggested in [32]. The ability to modify anisotropy by engineering the interface at atomic level makes the CoFeB/MgO heterostructure more versatile, as long as the interface roughness can be introduced in a well-controlled manner [33].

4. Conclusion

This paper presents an interface roughness model for the atomistic simulation of CoFeB/MgO heterostructure with CoFeB less than 2 nm in thickness. This thickness is essential to p-MTJs. The proposed model was validated using experimental values (from classic references) pertaining to the damping constant in p-MTJs. For a given roughness value, the damping constant can be calculated for films of various thickness using the seed point method. Our simulation results presented a very good fit with experimental results for the damping constant in thin films of less than 2 nm in thickness. Our model can also be used to characterize the effects of roughness on switching times and the energy barrier separating the two-magnetization directions. This model can also be used to explore atomic level phenomena in MRAM technology, which is beyond the limits of conventional micromagnetic simulations.

Data availability statement

The data that support the findings of this study are available upon reasonable request from the authors.

Acknowledgments

This work was financially supported by the 'Center for the Semiconductor Technology Research' from The Featured Areas Research Center Program within the framework of the Higher Education Sprout Project by the Ministry of Education (MOE) in Taiwan. Also supported in part by the Ministry of Science and Technology, Taiwan, under Grant MOST 110-2634-F-009-027/110-2622-8-009-018-SB.

ORCID iDs

Akhil K Ramesh https://orcid.org/0000-0003-1514-1271
Chih-Wei Cheng https://orcid.org/0000-0001-9743-9228
Vaibhav Rana https://orcid.org/0000-0001-8903-4431
Pratisha Gangwar https://orcid.org/0000-0003-4496-2861
Pushparaj Singh https://orcid.org/0000-0002-5894-7534
Yuan-Chieh Tseng https://orcid.org/0000-0001-5258-6152

References

[1] Dhull S, Nisar A and Kaushik B K 2021 *IEEE Trans. Nanotechnol.* **20** 653–61
[2] Nishioka K, Miura S, Honjo H, Inoue H, Watanabe T, Nasuno T, Naganuma H, Nguyen T, Noguchi Y and Yasuhira M 2021 *IEEE Trans. Electron Devices* **68** 2680–5
[3] Law W C and Wong S D W 2021 *Emerging Non-volatile Memory Technologies* (Berlin: Springer) pp 45–102
[4] Han S, Lee J, Suh K, Nam K, Jeong D, Oh S, Hwang S, Ji Y, Lee K and Song Y 2021 *(21-25 March 2021) IEEE Int. Reliability Physics Symp.* pp 1–5
[5] Han X, Wang X, Wan C, Yu G and Lv X 2021 *Appl. Phys. Lett.* **118** 120502
[6] Ramesh A K, Rana V, Das P and Singh P 2019 *IEEE 32nd Int. Conf. Micro Electro Mechanical Systems (MEMS)* pp 99–102
[7] Sun J, Brown S, Chen W, Delenia E, Gaidis M, Harms J, Hu G, Jiang X, Kilaru R and Kula W 2013 *Phys. Rev.* B **88** 104426
[8] Ikegawa S, Mancoff F B, Janesky J and Aggarwal S 2020 *IEEE Trans. Electron Devices* **67** 1407–19

[9] Endoh T and Honjo H 2018 *J. Low Power Electron. Appl.* **8** 44
[10] Sato H, Honjo H, Watanabe T, Niwa M, Koike H, Miura S, Saito T, Inoue H, Nasuno T and Tanigawa T 2018 *Int. Electron Devices Meeting* pp 27.2.1–27.2.4
[11] Honjo H, Sato H, Ikeda S, Sato S, Watanebe T, Miura S, Nasuno T, Noguchi Y, Yasuhira M and Tanigawa T 2015 *Symp. on VLSI Technology* pp 160–1
[12] Meo A, Visscher P, Chepulskyy R, Apalkov D, Chureemart J, Chureemart P, Chantrell R and Evans R 2021 *Phys. Rev.* B **103** 054426
[13] Ramesh A K, Chen K-M, Lin Y-J, Singh P, Wei J-H, Hsin Y-C, Wu C-I and Tseng Y-C 2021 *ACS Appl. Electron. Mater.* **3** 4047–55
[14] Sugihara A, Yakushiji K and Yuasa S 2019 *Appl. Phys. Express* **12** 023002
[15] Park H, Teramoto A, Tsuchimoto J-I, Hayashi M, Hashimoto K and Sugawa S 2019 *Jpn. J. Appl. Phys.* **58** SIIB29
[16] Nembach H, McMichael R, Schneider M, Shaw J and Silva T J 2021 *Appl. Phys. Lett.* **118** 012408
[17] Evans R F, Fan W J, Chureemart P, Ostler T A, Ellis M O and Chantrell R W 2014 *J. Phys.: Condens. Matter* **26** 103202
[18] Shen W, Mazumdar D, Zou X, Liu X, Schrag B and Xiao G 2006 *Appl. Phys. Lett.* **88** 182508
[19] Liu X, Zhang W, Carter M J and Xiao G 2011 *J. Appl. Phys.* **110** 033910
[20] Li X-J, Jiang S-L, Zhang J-Y, Liu Q-Q, Liu Y-W, Zhao J-C, Wu Z-L, Feng C, Li M-H and Yu G-H 2016 *Appl. Surf. Sci.* **365** 275–9
[21] Chureemart J, Chantrell R W, Chepulskyy R, Wang S, Apalkov D, Evans R F and Chureemart P 2019 *Phys. Rev. Appl.* **11** 044001
[22] Evans R, Bate D, Chantrell R, Yanes R and Chubykalo-Fesenko O 2011 *Phys. Rev.* B **84** 092404
[23] Ikeda S, Miura K, Yamamoto H, Mizunuma K, Gan H, Endo M, Kanai S, Hayakawa J, Matsukura F and Ohno H 2010 *Nat. Mater.* **9** 721–4
[24] Ellis M O, Evans R F, Ostler T A, Barker J, Atxitia U, Chubykalo-Fesenko O and Chantrell R W 2015 *Low Temp. Phys.* **41** 705–12
[25] Sato H, Chureemart P, Matsukura F, Chantrell R W, Ohno H and Evans R F L 2018 *Phys. Rev.* B **98** 214428
[26] Bowden G, Stenning G and van der Laan G 2016 *J. Phys.: Condens. Matter* **28** 066001
[27] Asselin P, Evans R F L, Barker J, Chantrell R W, Yanes R, Chubykalo-Fesenko O, Hinzke D and Nowak U 2010 *Phys. Rev.* B **82** 054415
[28] Donahue M J and Porter D G 1999 OOMMF user's guide, version 1.0 interagency report NISTIR 6376 (National Institute of Standards and Technology)
[29] Lone A H, Shringi S, Mishra K and Srinivasan S 2020 *IEEE Trans. Magn.* **57** 4400410
[30] Pathak S, Cha J, Jo K, Yoon H and Hong J 2017 *Appl. Phys. Lett.* **110** 232401
[31] Slonczewski J C 1996 *J. Magn. Magn. Mater.* **159** L1–L7
[32] Sun Y, Gong J, Deng Z, Chen R and Meng F 2021 *ACS Appl. Electron. Mater.* **3** 5423–32
[33] Rana B and Otani Y 2019 *Commun. Phys.* **2** 1–12